



## Full Length Article

# Underground coal gasification – A numerical approach to study the formation of syngas and its reactive transport in the surrounding strata

Renato Zagorščak<sup>a</sup>, Ni An<sup>a,\*</sup>, Rupesh Palange<sup>b</sup>, Michael Green<sup>c</sup>, Murugesan Krishnan<sup>b</sup>, Hywel Rhys Thomas<sup>a</sup>

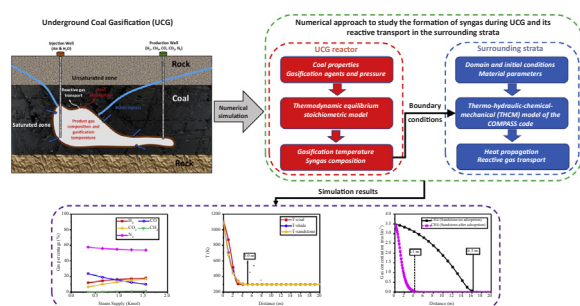
<sup>a</sup> Geoenvironmental Research Centre (GRC), Cardiff School of Engineering, Cardiff University, Cardiff, Wales, UK

<sup>b</sup> Department of Mechanical and Industrial Engineering, Indian Institute of Technology Roorkee, Roorkee, India

<sup>c</sup> UCG Engineering Ltd, UK, Surbiton, Surrey KT6 6QB, UK



## GRAPHICAL ABSTRACT



## ARTICLE INFO

## Keywords:

Energy  
Underground coal gasification  
Equilibrium model  
Coupled modelling  
Gas flow  
Sorption

## ABSTRACT

In this work, a method to study the formation of syngas during the underground coal gasification (UCG) process and its reactive transport in the surrounding strata is proposed. It combines a thermodynamic equilibrium stoichiometric model of the cavity reactions with a coupled thermo-hydraulic-chemical-mechanical (THCM) framework of COMPASS code for the transport of UCG products away from the cavity. With the input information of coal properties obtained from the South Wales coalfield, gasification reagents (air and steam) and thermodynamic conditions (initial temperature and pressure), the thermodynamic equilibrium model developed provides the maximum yield of gasification products and temperature from a UCG system. Gasification results giving the syngas composition with the highest percentage of methane and carbon dioxide, are then used as the chemical (gas) and thermal boundary conditions for the coupled thermo-chemical model of the THCM framework to analyse the variations of temperature and gas concentrations, in strata surrounding the UCG reactor. For that purpose, a set of numerical simulations considering three porous media (coal, shale and sandstone) with different physico-chemical properties is conducted. The gasification results demonstrate that increasing the amount of steam injected in the UCG reactor decreases the temperature of the system as well as the concentration of carbon monoxide and nitrogen, while benefiting the production of hydrogen, methane and carbon dioxide. The numerical simulations performed using the THCM model indicate that multicomponent gas diffusion and advection are competing transport mechanisms in porous media with intrinsic permeability higher than 1 mD (sandstone), while the gas diffusion becomes a dominant transport process in porous media with an intrinsic permeability lower than 1 mD (coal and shale). Moreover, the simulation results of reactive transport of methane and carbon dioxide in different porous media demonstrate the significance of considering the

\* Corresponding author at: Geoenvironmental Research Centre (GRC), Cardiff School of Engineering, Cardiff University, Queen's Buildings, The Parade, Cardiff CF24 3AA, Wales, UK.

E-mail address: [aAnn@cardiff.ac.uk](mailto:aAnn@cardiff.ac.uk) (N. An).

<https://doi.org/10.1016/j.fuel.2019.04.164>

Received 28 September 2018; Received in revised form 5 April 2019; Accepted 30 April 2019

Available online 13 May 2019

0016-2361/ © 2019 Elsevier Ltd. All rights reserved.

adsorption effect in the gas transport in the overall UCG process. In particular, the retardation of the gas front due to gas sorption is the most pronounced in coal, followed by shale and then sandstone. In conclusion, the model presented in this study demonstrates its potential application in managing the environmental practices, reducing pollution risk and securing greater public and regulatory support for UCG technology.

## 1. Introduction

Coal reserves significantly exceed those of oil and gas, however less than one-sixth of the world's coal is currently economically accessible using conventional mining methods [1]. Underground coal gasification (UCG) is a process whereby coal deposits that are either too deep underground or too costly to be extracted using traditional mining techniques, are converted into a combustible gas, commonly known as syngas. A UCG operation consists of a series of injection and production wells drilled into a coal seam where reactant gases, i.e. air, oxygen or steam, are supplied (Fig. 1). As having a fully instrumented UCG trial with comprehensive data extraction is challenging and expensive, computational modelling offers an inexpensive way for predicting the complex interaction of various processes involved during and beyond the UCG operation.

An extensive literature review given in Khan et al. [2] and Perkins [3], suggests that current numerical models predominantly focus on the phenomena of coal gasification and cavity formation [3], the product gas compositions and quality [4–6], underlying thermo/mechanical/chemical reactions and heat and mass transport phenomena in the permeable bed and newly formed cavity [7–12]. Those numerical models are then applied to predict the effect of various physical and operating parameters on the performance of the UCG process and provide suggestions for the economic and technical feasibility of UCG technology. For instance, an innovative thermodynamic underground coal gasification model was proposed firstly by Klebingat et al. [12] to optimize the coupled synthesis gas quality and simultaneously reduce tar yields under given geological boundary conditions and then applied further by Klebingat et al. [13] to provide a predictive UCG analysis taking into account tar production control and economic gas quality constraints to achieve optimum operating options in view of synthesis gas quality and reduced tar production. Other models focus on the geo-mechanical phenomena in the surrounding strata dealing with the stress-strain changes as a result of thermo-mechanical induced effects and potential surface subsidence changes [14,15].

Besides primary gas components, i.e. methane, hydrogen, carbon monoxide and carbon dioxide, a number of organic and inorganic contaminants, such as phenols, benzene, sulphates, metal and metalloid elements can be generated and released during the UCG process [16]. The UCG has been performed in over 75 trials throughout the world, and despite most of the UCG trials not experiencing significant environmental issues, potential pollution is the biggest public and regulatory concern [17]. Several researchers who focused on the generation and transport of contaminants via experimental and numerical analyses [18–25] have suggested that operating the UCG process above the hydrostatic pressure can pose an environmental concern due to the chemical reactions in the groundwater environment depending on mineral composition, temperature, concentration of syngas components and the chemical composition of groundwater. However, modelling of contaminant transport and reactions received less attention as it is a complex process with multiple aspects involving heat, mass, stress-strain and physico-chemical reactions [18,26]. For example, little is known of how the gas sorption affects the gas migration around the UCG cavity and whether it can help to retard potential gas leakage. Upadhye et al. [27] concluded that general hydrogeological models are not appropriate for predictions and assessments related to groundwater pollution and environmental issues in the context of UCG as such models often do not include the complexity of the processes and effects involved in UCG. Therefore, modelling platforms possible to

simultaneously simulate the production of syngas, the environmental impact of UCG products both in liquid and gaseous state and the geo-mechanical impacts of the UCG in complex multi-well configurations are therefore required to enhance the understanding of all the environmental aspects related to UCG [3]. Performing such work is also crucial in order to demonstrate to the regulatory bodies and the public under which conditions UCG can be feasible without generating environmental damage and pollution.

In this paper, a comprehensive thermodynamic and coupled thermo-hydro-chemical-mechanical (THCM) modelling approach is presented. Through specific process parameters, a thermodynamic equilibrium stoichiometric model for calculating syngas concentrations and reaction temperature has been coupled with the existing THCM framework of the COMPASS software which has a background of high-performance simulations of three-dimensional multiphase, multi-component reactive transport in porous geomaterials [28–30]. The developed model is then applied to investigate the gas migration and the effect of its sorption on transport through different geological media (coal, shale and sandstone) surrounding the UCG cavity, considering the scenario of potential syngas leakage.

## 2. Theoretical framework

In this section, a theoretical framework is presented consisting of a thermodynamic equilibrium stoichiometric model and a coupled thermo-chemical model contained within the thermo-hydraulic-chemical-mechanical framework of the COMPASS Code (Fig. 2). The thermodynamic equilibrium model has been developed based on the previous work on biomass and coal gasification [31,32] and is being incorporated within the COMPASS framework through the boundary condition interface, i.e. the results of individual syngas concentrations and the reactor temperature serve as an input for the reactive transport modelling. The COMPASS code is a coupled thermo-hydro-chemical-mechanical model, previously developed at the Geo-environmental Research Centre by Thomas and co-workers [28–30,33,34] to address various geo-environmental issues. COMPASS is based on a theoretical formulation that can be described as a mechanistic approach. The various mechanisms of behaviour are included in an additive manner with inter-related couplings being accommodated. The model is based on mass conservation for moisture, gas and chemical transport and energy equation for the heat transfer. Mechanical behaviour is also included via an appropriate constitutive relationship using the elastoplastic approach.

The COMPASS code has been successfully extended by including the

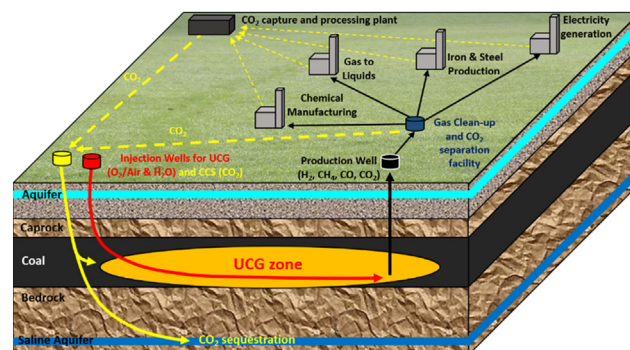


Fig. 1. Schematic diagram of the overall UCG process.

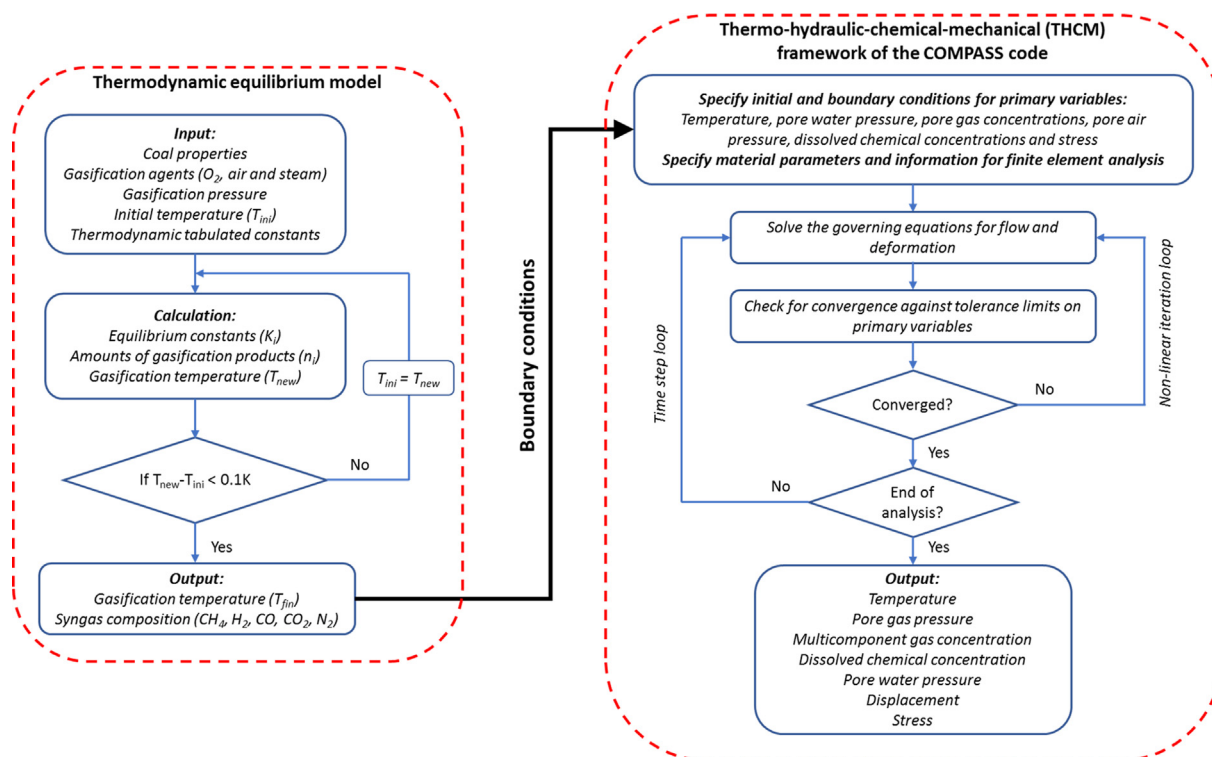


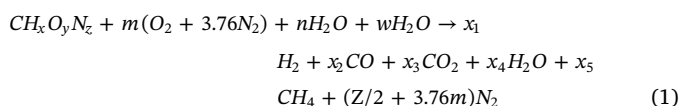
Fig. 2. Numerical approach consisting of a thermodynamic equilibrium stoichiometric model and a coupled thermo-hydraulic-chemical-mechanical framework of the COMPASS code.

advanced geochemical model PHREEQC (version 2) [35]. Through both equilibrium and kinetically controlled geochemical reactions, the model is capable to simulate the reactive transport and fate of multi-component and dissolved chemicals and gases. The geochemical reactions considered in the coupled model include phase transformation, ion exchange, precipitation and dissolution of minerals, surface complexation and redox reactions. The transport model (COMPASS) and the geochemical model (PHREEQC) are linked together using a sequential non-iterative approach [29]. Further details of the applied models are provided in the following sections.

### 2.1. Thermodynamic model

The production of syngas using gasification is a complex process that depends on several factors including the composition of feedstock, the gasifier conditions, temperature and pressure, and the type and amount of oxidiser and moderator. A thermodynamic equilibrium modelling approach is widely used to evaluate the performance of gasification systems in terms of product gas composition and efficiency [31,32].

The global gasification reaction for one mole of feedstock can be represented as:



where  $CH_xO_yN_z$  is the chemical formula for the feedstock/coal, subscripts  $x$ ,  $y$  and  $z$  are the number of moles of hydrogen, oxygen, nitrogen in feedstock per mole of carbon,  $n$  represents the amount of moisture per mole of feedstock,  $m$  represents the amount of air supply per mole of feedstock and  $w$  represents the amount of steam supply in mole per mole of feedstock. The coefficients  $x_1$ ,  $x_2$ ,  $x_3$ ,  $x_4$ ,  $x_5$  represent the number of moles of  $H_2$ ,  $CO$ ,  $CO_2$ ,  $H_2O$  and  $CH_4$ , respectively. The molar concentrations of syngas products and gasification temperature

together comprise of six unknowns and are output data from the model. Hence, six equations are required to determine six unknowns, three of which will be obtained from the mass balance for the global gasification reaction.

Carbon balance gives:

$$x_2 + x_3 + x_5 = 1 \quad (2)$$

Hydrogen balance gives:

$$2x_1 + 2x_4 + 4x_5 = x + 2n + 2w \quad (3)$$

Oxygen balance gives:

$$x_2 + 2x_3 + x_4 = y + 2m + n + w \quad (4)$$

To obtain the remaining equations, chemical reactions as an integral part of the gasification process are used. By combining the Boudouard reaction and the water-gas reaction, the water-gas shift reaction can be obtained and is given as [36]:



Methanation reaction gives:



The equilibrium constant for the water-gas shift reaction is:

$$K_1 = \frac{x_1x_3}{x_2x_4} \quad (7)$$

The equilibrium constant for the methanation reaction is:

$$K_2 = \frac{x_5}{x_1^2} \left( \frac{P}{x_T P_0} \right)^{-1} \quad (8)$$

where  $x_T$  is the total sum of all the product gaseous species,  $P$  is the pressure and  $P_0$  is the standard reference state pressure.

In order to solve the non-linear equations (7) and (8), the values of the reaction constants must be calculated using the following equation:

$$\ln K_i = \frac{-\Delta G^0}{RT} \quad (9)$$

where  $R$  is the universal gas constant and  $\Delta G^0$  is the standard Gibbs function at a given temperature  $T$ .

The dependence of  $\Delta G^0$  on temperature can be expressed through heat of formation which is further expanded in terms of specific constants as [37]:

$$\frac{d\ln K}{dT} = \frac{\Delta H^0}{RT^2} \quad (10)$$

$$\frac{\Delta H^0}{R} = \frac{J}{R} + (\Delta A)T + \frac{\Delta B}{2}T^2 + \frac{\Delta C}{3}T^3 - \frac{\Delta D}{T} \quad (11)$$

Substituting Eq. (11) in (10) and integrating we get,

$$\ln K = \frac{-J}{RT} + \Delta A \ln T + \frac{\Delta B}{2}T + \frac{\Delta C}{6}T^2 + \frac{\Delta D}{2T^2} + I \quad (12)$$

From Eqs. (9) and (12) the dependence of  $\Delta G$  on temperature can be written as:

$$\Delta G^0 = J - RT \left( \Delta A \ln T + \frac{\Delta B}{2}T + \frac{\Delta C}{6}T^2 + \frac{\Delta D}{2T^2} + I \right) \quad (13)$$

where the data for constants  $\Delta A$ ,  $\Delta B$ ,  $\Delta C$ ,  $\Delta D$  can be obtained from [38]. The constants  $J$  and  $I$  are calculated from Eqs. (11) and (13) at temperature of 298 K.

By incorporating the tabulated values and constants the expression for equilibrium constants obtained are:

$$\ln K_1 = \frac{5872.39}{T} + 1.86 \ln T - 2.7 \times 10^{-4}T - \frac{58200}{T^2} - 18.01 \quad (14)$$

$$\ln K_2 = \frac{7083.41}{T} - 6.567 \ln T + 3.733 \times 10^{-3}T - 3.6 \times 10^{-7} + \frac{35050}{T^2} + 32.5 \quad (15)$$

To obtain the gasification temperature, the energy balance is used:

$$\begin{aligned} \Delta h_{f, \text{feedstock}} + n h_{f, \text{H}_2\text{O}}^0 + w h_{f, \text{H}_2\text{O}}^0 + m h_{f, \text{O}_2}^0 + 3.76 m h_{f, \text{N}_2}^0 \\ = x_1 (h_{f, \text{H}_2}^0 + C_{p, \text{H}_2} \Delta T) + x_2 (h_{f, \text{CO}}^0 + C_{p, \text{CO}} \Delta T) + x_3 \\ (h_{f, \text{CO}_2}^0 + C_{p, \text{CO}_2} \Delta T) + x_4 (h_{f, \text{H}_2\text{O}}^0 + C_{p, \text{H}_2\text{O}} \Delta T) + x_5 \\ (h_{f, \text{CH}_4}^0 + C_{p, \text{CH}_4} \Delta T) + (z/2 + 3.76m) (h_{f, \text{N}_2}^0 + C_{p, \text{N}_2} \Delta T) \end{aligned} \quad (16)$$

where  $h_f$  is the enthalpy of formation and  $\Delta T = T - T_{\text{ref}}$  where  $T_{\text{ref}}$  is 298 K.

The data for heat of formation of all the species involved in Eq. (16) can be obtained from JANAF thermochemical tables [39]. The specific heat,  $C_p$ , as a function of temperature can be expressed as [38]:

$$C_p = R \left[ A + B T_{\text{av}} + \frac{C}{3} (4 T_{\text{av}}^2 - T_{\text{ref}} T) + \frac{D}{T_{\text{ref}} T} \right] \quad (17)$$

where  $A$ ,  $B$ ,  $C$ ,  $D$  are tabular values and  $T_{\text{av}} = (T_{\text{ref}} + T)/2$ .

The model was developed in FORTRAN programming language, with the solution of the non-linear equations being achieved using the Newton-Raphson method. The solution procedure for the thermodynamic equilibrium model can be found in Jarunthammachote and Dutta [31].

### 2.1.1. Verification and validation

For the verification exercise, the results of syngas composition of the present model are compared with the results of the numerical model developed by Jarunthammachote and Dutta [31] for gasification of rubber wood as a biomass feedstock. The comparison is made by setting the gasification temperature fixed at 1100 K for moisture contents of 16% and 14% with air supply rates of 0.4647 and 0.4591 kmole per kmole of biomass, respectively. Fig. 3 shows that the results from both models are in excellent agreement with each other. This consolidates

the accuracy of the computational algorithm developed for thermodynamic equilibrium model for gasification.

The model is further compared with the experimental data on gasification of lignite reported by Patel et al. [36]. The results obtained are for air supply of 0.45 kmole at a fixed gasification temperature of 1100 K. Fig. 4 shows reasonable agreement with the results of the model and the experimental data. The slight deviation in results can be attributed to assumptions such as ideal gas behaviour, modelling of different reaction zones as a single zone, absence of tar etc. The lower concentration of methane is because the methanation reaction does not reach equilibrium at higher temperatures.

### 2.2. COMPASS code

The governing equations of the coupled thermal, hydraulic, chemical and mechanical framework of the COMPASS code to study the behaviour of unsaturated soils have already been provided elsewhere [28,29,33,40]. Furthermore, the governing equations for the reactive transport of multicomponent gas in a single porosity unsaturated medium have been given in Sedighi et al. [41], assuming an ideal gas behaviour. Hosking et al. [30] presented the governing equations for multicomponent reactive chemical transport in dual porosity geomaterials as well as the aspects related to non-ideal gas flow at high pressures.

For the purpose of this work, a coupled thermal-chemical model of the COMPASS framework has been used. The existing thermal model was further extended to incorporate temperature dependence of gas conductivity as well as to consider the variations of thermal

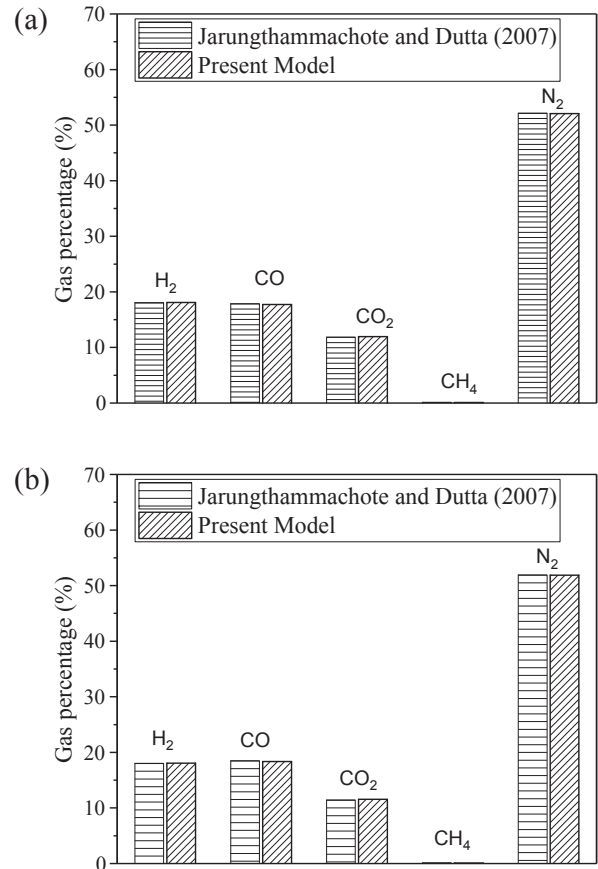


Fig. 3. Comparison of the results obtained using the developed model with the model developed by Jarunthammachote et al. [31] for different air to fuel ratios and moisture contents in rubber wood at a fixed temperature of 1100 K: (a)  $m = 0.4647$ , moisture content = 16%; (b)  $m = 0.4591$ , moisture content = 14%



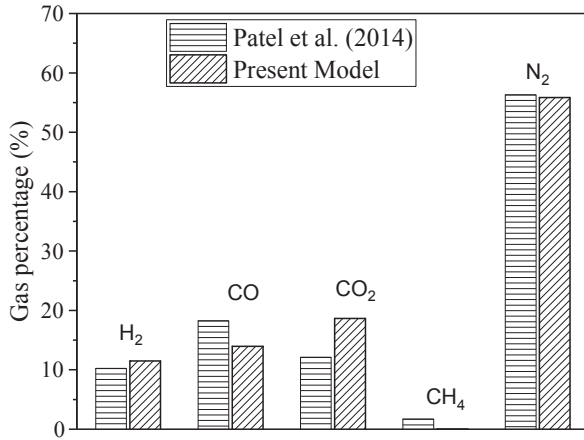


Fig. 4. Comparison of the results using the developed model with the experimental results by Patel et al. [36] for gasification of lignite.

conductivity and heat capacity with temperature of different porous media adopted in this study. Furthermore, geochemical reactions are included via the sorption/desorption module of the COMPASS code to study the effect of sorption on gas transport.

The governing equation of heat transfer has been developed based on the energy conservation law in

$$\frac{\partial}{\partial t} [H_c (T - T_R)] = -\nabla \lambda_T \nabla T \quad (18)$$

where  $H_c$  is the heat storage capacity,  $T$  is the soil/rock temperature,  $T_R$  is a reference temperature, and  $\lambda_T$  is the thermal conductivity. Heat convection is neglected in this work due to the dominate role of heat conduction in low permeability medium [42].

A mass conservation equation is applied to derive the multi-component gas chemical transport in which the temporal derivative of the gas chemical accumulation is equal to the spatial gradient of the flux. A sink/source term is added allowing for chemical reactions. The governing equation is given by:

$$\frac{\partial}{\partial t} [\theta c_g^i] + R^i = -\nabla [c_g^i v_g] + \nabla [D^i \nabla c_g^i] \quad (19)$$

where  $c_g^i$  is the  $i^{\text{th}}$  gaseous chemical component and  $D^i$  is the effective diffusion coefficient derived from the free fluid diffusion coefficient to account for the tortuous diffusion paths in a porous medium [30].  $\theta$  is the volumetric gas content represented by multiplying porosity  $n$  and degree of gas saturation  $S_g$ .

Using Darcy's law for the advective flux, the expression for  $v_g$  is:

$$v_g = -k \left[ \nabla \frac{u_g}{\rho_g g} + \nabla z \right] \quad (20)$$

where  $z$  is the elevation and  $k$  is the gas conductivity which can be expanded to give:

$$k = \frac{K \rho_g g}{\mu_g} \quad (21)$$

where  $K$  is the intrinsic permeability and  $\mu_g$  is the absolute gas viscosity which is included using the approach in which viscosity depends on composition, temperature and pressure [30]. The viscosity model is expressed as:

$$\mu_g = 0.1 [f(\mu_g^0) + \mu_g^D] \quad (22)$$

where  $f(\mu_g^0)$  is a function of the gas mixture viscosity at low pressure and  $\mu_g^D$  is an adjustment for dense gases.

The bulk gas pressure,  $u_g$ , can be expressed in terms of the sum of concentrations of the chemical components in the gas phase, given by:

$$u_g = ZRT \sum_{j=1}^{n_g} c_g^j \quad (23)$$

where  $Z$  is the compressibility factor (equal to 1 in ideal gas case),  $R$  is the universal gas constant,  $T$  is the temperature, and  $n_g$  is the number of gas components.

Development of a sink/source term for chemical reactions,  $R^i$ , is limited here to adsorption and desorption of gases by solids and can be expressed as:

$$R^i = \rho_s \frac{\partial s^i}{\partial t} \quad (24)$$

where  $\rho_s$  is the dry bulk density of the solid and  $s^i$  is the adsorbed amount of the  $i^{\text{th}}$  chemical component which has been calculated using the extended Langmuir isotherm [30]:

$$s^i = \frac{n^i b_L^i ZRT c_g^i}{1 + ZRT \sum_{j=1}^{n_g} b_L^j c_g^j} \quad (25)$$

where  $n^i$  is the Langmuir capacity and  $b_L^i$  is the reciprocal of the Langmuir pressure. In this approach, it is assumed that the sorption process is sufficiently fast compared to the transport speed. Hence, the local chemical equilibrium between the adsorbed gas phase and the free gas phase is considered to exist.

A numerical solution of the two governing partial differential equations is achieved with the finite element method for spatial discretisation and the finite difference method for temporal discretisation [28,29,33,40]. The THCM model of the COMPASS code has been extensively verified, validated and applied for a range of geo-environmental/geo-energy applications. In regards to the thermo-chemical model used in this work, the thermal aspects of the model have been verified against analytical solutions and validated against experimental data on heat propagation in various types of soils and rocks [34,43,44]. Also, the multicomponent high pressure ideal and real gas transport and its sorption in coal have been verified against analytical solutions for pure diffusive and advective-diffusive gas transport as well as the comparison of simulation results with those presented in the literature for an alternative numerical model and validated against experimental data [30,45]. Details of the numerical formulation and computational aspects have been discussed in previous publications mentioned above and therefore, the details are not repeated here.

### 3. Problem setup

During underground coal gasification, the process gas will tend to escape from the cavity if there is an outward pressure gradient. In order to prevent this, a common practice is to ensure that the fluid flow from the strata surrounding the cavity must be towards it [46]. However, under specific conditions where coal acts as a confined aquifer surrounded by low permeability strata, a layer of unreacted coal may exist around the upper part of the cavity where the surrounding coal drains off water and the pores are partially filled with gas [46]. This is schematically shown in Fig. 5. The zone of unreacted coal could be extended even further in dipping coal seams where the gas could flow a long distance in the up-dip direction [46].

This work is therefore trying to provide further understanding of how the amount of water injected into the cavity affects the concentration of the individual syngas components and the reaction temperature. Furthermore, it is studied how the primary product gases, i.e. methane, hydrogen, carbon monoxide, carbon dioxide and nitrogen, flow through the overlying strata. As methane and carbon dioxide are very potent greenhouse gases, it is also investigated whether sorption of these gases on the surrounding rock, upon their potential escape from the cavity, can retard their propagation and provide a potential for their storage.

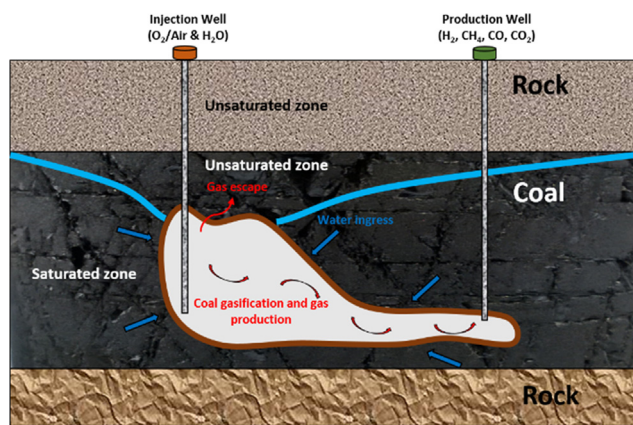


Fig. 5. Potential of gas escape where a shoulder of unreacted coal may exist in the upper part of the coal seam surrounding the cavity (adapted from Camp and White [46]).

### 3.1. Domain and material properties

Coal seams are often overlaid by low permeable rocks such as shales and mudstones, and more permeable sandstones which is also the case for the South Wales Coalfield [47]. A recent study of the South Wales coalfield through exploratory drilling for environmental monitoring purposes has suggested that samples from various depths exhibit mineralogical characteristics of shale deposits and that several thick coal seams are overlaid by sandstone layers [48]. Furthermore, through continuous monitoring of ground water level in the boreholes in a duration of more than 2.5 years, it was shown that the water level in one of the boreholes is around 350 m below the surface [48]. Therefore, a sensitivity analysis considering gas flow through mudstone/shale, sandstone and coal in partially dry conditions, assuming the degree of water saturation of 0.61 as a reasonable value for the materials studied [49–51], has been considered in this study to reflect the real geological conditions experienced in the coalfield.

The system is represented as a 30 m long domain with 1 m height, discretised into 300 equally-sized 4-noded quadrilateral elements. A summary of the material parameters is given in Table 1. As shown in the table, thermal conductivity and heat capacity of the materials studied have been considered as a function of temperature. Several studies conducted analyses of gas sorption in porous geo-materials over a range of temperatures, on coals up to 350 K [52] and shales up to 318 K [53], and have suggested that the sorption capacity decreases with an increase in temperature as the sorption is an exothermic process [52,53]. However, literature data on the sorption of different gases under high-temperature conditions that can be experienced in the surroundings of the UCG cavity is very scarce. Hence, in this work the sorption properties of different materials represent sorption at isothermal conditions. Sorption data at the temperature of 313 K and 318 K are adopted for the cases of CO<sub>2</sub> and CH<sub>4</sub> on coal, respectively. Sorption of the same gases on shale is taken at 318 K, while the sorption of CO<sub>2</sub> and CH<sub>4</sub> on

Table 1  
Parameter values used in simulations.

Material parameters	Sandstone	Coal	Shale/Mudstone
Porosity [%]	25 [55]	25 [56]	25 [57]
Permeability [mD]	1.0 [58]	0.1 [34]	0.01 [57]
Density [kg.m <sup>-3</sup> ]	2650 [58]	1376 [34]	2316 [59]
Thermal conductivity [W.m <sup>-1</sup> .K <sup>-1</sup> ]	$\lambda = 1/(0.000497 * T + 0.764518)$ [60]	$\lambda = 3 * 10^{-6} * T^2 - 0.001 * T + 0.2625$ [61]	$\lambda = 1/(0.000288 * T + 0.749849)$ [60]
Heat capacity [J.kg <sup>-1</sup> .K <sup>-1</sup> ]	810 [60]	$C_p = -0.001 * T^2 + 2.1418 * T + 854.83$ [61]	$C_p = 0.0007 * T^2 - 1.1434 * T + 1336$ [60]
Langmuir pressure (CO <sub>2</sub> ) [MPa]	2.83 [62]	0.61 [54]	1.0 [53]
Langmuir capacity (CO <sub>2</sub> ) [mol/kg]	0.49 [62]	1.73 [54]	0.285 [53]
Langmuir pressure (CH <sub>4</sub> ) [MPa]	3.86 [63]	1.2 [52]	1.71 [53]
Langmuir capacity (CH <sub>4</sub> ) [mol/kg]	0.175 [63]	1.52 [52]	0.184 [53]

Table 2

Proximate and ultimate characteristics of coal considered in the model simulations [54]

Proximate analysis		Ultimate analysis	
Moisture content	0.91%	Total carbon content	89.5%
Ash	4.62%	Sulphur content	0.87%
Volatile matter	5.73%	Hydrogen content	3.16%
Fixed carbon content	88.7%	Nitrogen content	1.31%
		Oxygen content	0.33%

sandstone is represented at 323 K and 296 K, respectively. It should be noted that the sorption parameters for shale and sandstone were obtained by fitting the Langmuir curve to the experimental data provided in the literature (Table 1).

### 3.2. Model parametrization and boundary conditions

The thermodynamic equilibrium model is used to analyse the effect of steam supply ranging from 0.35 to 1.55 kmol on the product gas composition and the reaction temperature. Furthermore, air is considered to be a primary gasifying agent at a constant injection of 0.5 kmol. Coal properties of an anthracite coal from the South Wales coalfield have been used as an input for the thermodynamic equilibrium model. For that purpose, Proximate and ultimate analysis data given in Table 2 have been used [54].

Based on the results provided by the thermodynamic equilibrium model, a scenario generating the highest amount of CO<sub>2</sub> and CH<sub>4</sub> is used as input, i.e. boundary condition for the reactive transport model of the COMPASS code. Initial and downstream boundary conditions are assumed to be atmospheric. The simulation considered an arbitrary injection pressure of 20 bar which would represent UCG at a minimum depth of 200 m below ground level. The simulation period is 30 days.

## 4. Results and discussion

In this section, the simulation results on gasification temperature and syngas formation as well as heat and gas propagation through different porous media obtained using the thermo-chemical model of the COMPASS code are presented. Subsequently, the results on gas propagation in the same porous media are shown and analysed with emphasis on the effect of gas sorption on gas transport.

### 4.1. Reactive transport boundary conditions

The results of the thermodynamic model are given in Figs. 6 and 7. It is shown in Fig. 6 that steam supply affects the gasification temperature, i.e. increase in the amount of steam submitted to the system decreases the temperature in the UCG cavity by 115 K, i.e. from 1224 K to 1109 K for the range of the steam supply considered. This is related to the fact that steam gasification is a highly endothermic reaction which favours the generation of hydrogen. This can be confirmed from

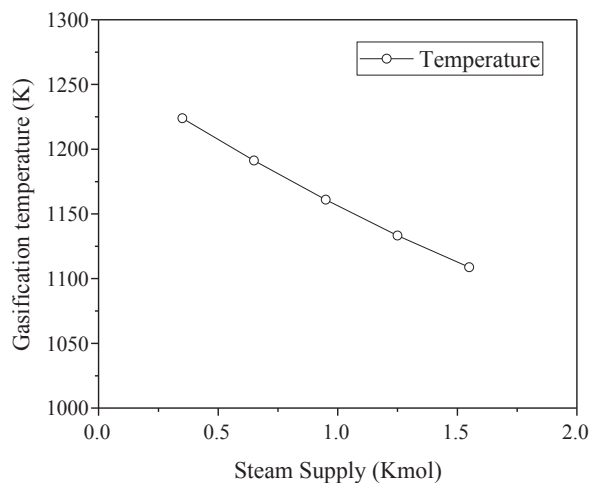


Fig. 6. The effect of steam supply on the gasification temperature.

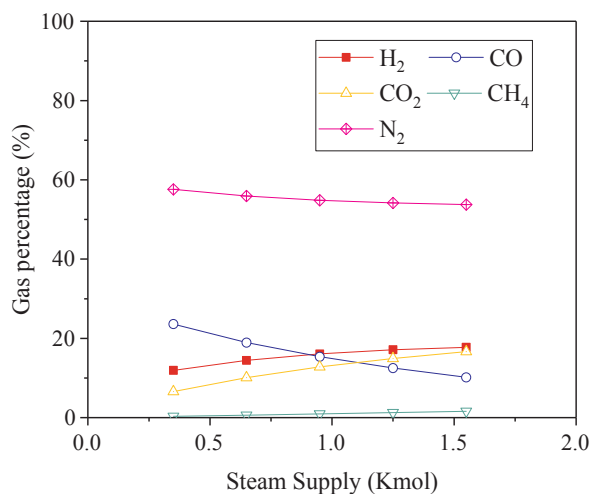


Fig. 7. The effect of steam supply on the syngas composition (on dry basis).

Fig. 7 where it is visible that an increase in steam supply benefits the hydrogen and methane production, while it reduces the concentration of carbon monoxide generated. In particular, the concentration of hydrogen increases from 11.9% to 17.75%, concentration of methane from 0.35% to 1.62% and concentration of carbon monoxide decreases from 23.59% to 10.17%.

However, the CO<sub>2</sub> concentration increases from 6.57% to 16.68%. Hence, small amounts of steam injection should be encouraged since net calorific value of syngas increases based on increase in yield of H<sub>2</sub> and CH<sub>4</sub>. Higher methane yield is obtained if gasification takes place at lower temperatures and higher pressure. Higher amounts, then considered in this study, of steam injection should be avoided owing to drop in CO and increase in CO<sub>2</sub> concentration. As mentioned, the

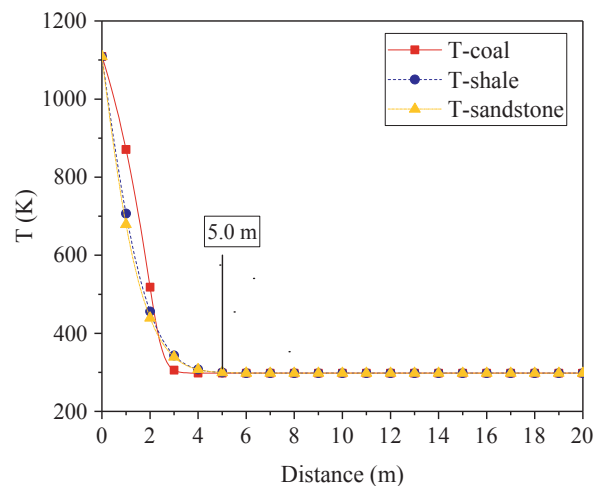


Fig. 8. The distribution of temperature after 30 days in different porous media.

simulation results providing the highest amounts of CO<sub>2</sub> (16.68%) and CH<sub>4</sub> (1.62%) as well as the corresponding gasification temperature of 1108.75 K are used as boundary conditions for the reactive transport model to analyse the heat and gas propagation in different porous media surrounding the UCG cavity. A complete overview of the reactive transport boundary conditions is given in Table 3.

#### 4.2. Heat transport

Fig. 8 shows the temperature distribution in the domain at the end of the studied period. It can be observed that for the different geological formations considered in this study, the influenced areas of temperature are limited to round 5.0 m. As the heat transfer in this work was governed by conduction only, some minor differences can be observed due to the different thermal conductivities and heat capacities of three materials considered in this study, as indicated in Table 1.

#### 4.3. Gas propagation

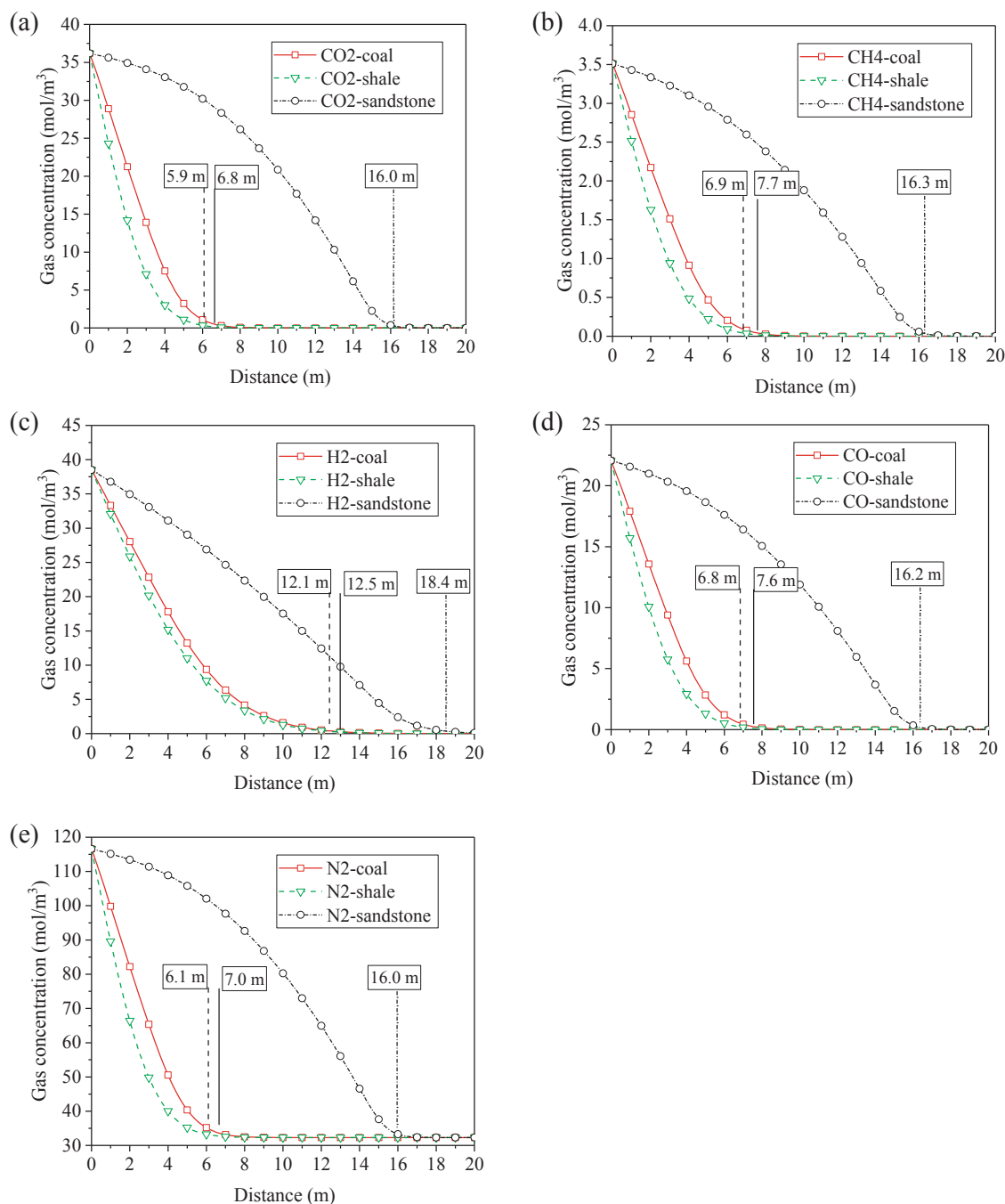
The propagation of syngas components in different porous media at the end of the studied period is given in Fig. 9, where the transport of CO<sub>2</sub>, CH<sub>4</sub>, H<sub>2</sub>, CO and N<sub>2</sub> is presented in Fig. 9a, 9b, 9c, 9d and 9e, respectively.

Fig. 9a shows that CO<sub>2</sub> reaches the distance of 16.0 m in sandstone, which is further in comparison to gas propagation up to 6.8 m in coal and 5.9 m in shale. For other gases studied in Fig. 9b, 9c, 9d and 9e, it can also be observed that the gas front in the sandstone is located further than in coal and shale. In addition, the gas front of CO<sub>2</sub>, CH<sub>4</sub>, CO and N<sub>2</sub> is minimum 8.6 m and 5.9 m for H<sub>2</sub> further in sandstone compared to other materials (coal and shale). Such observation is mainly related to the difference in intrinsic permeabilities of different porous media (sandstone 1 mD > coal 0.1 mD > shale 0.01 mD), leading to the differences of gas conductivities which controls the gas advection in

Table 3

Reactive transport boundary conditions.

Upstream boundary conditions	Initial conditions	Downstream boundary conditions
Fixed gas concentrations at 20 bar: $C_g(\text{CO}_2) = 36.19 \text{ mol.m}^{-3}$ $C_g(\text{CH}_4) = 3.51 \text{ mol.m}^{-3}$ $C_g(\text{H}_2) = 38.51 \text{ mol.m}^{-3}$ $C_g(\text{CO}) = 22.06 \text{ mol.m}^{-3}$ $C_g(\text{N}_2) = 116.59 \text{ mol.m}^{-3}$	Initial gas concentrations at 1 bar: $C_g(\text{CO}_2) = 0 \text{ mol.m}^{-3}$ $C_g(\text{CH}_4) = 0 \text{ mol.m}^{-3}$ $C_g(\text{H}_2) = 0 \text{ mol.m}^{-3}$ $C_g(\text{CO}) = 0 \text{ mol.m}^{-3}$ $C_g(\text{N}_2) = 32.31 \text{ mol.m}^{-3}$ $C_g(\text{O}_2) = 8.59 \text{ mol.m}^{-3}$ Initial temperature: $T = 298 \text{ K}$	Fixed gas concentrations at 1 bar: $C_g(\text{CO}_2) = 0 \text{ mol.m}^{-3}$ $C_g(\text{CH}_4) = 0 \text{ mol.m}^{-3}$ $C_g(\text{H}_2) = 0 \text{ mol.m}^{-3}$ $C_g(\text{CO}) = 0 \text{ mol.m}^{-3}$ $C_g(\text{N}_2) = 32.31 \text{ mol.m}^{-3}$ $C_g(\text{O}_2) = 8.59 \text{ mol.m}^{-3}$ Fixed temperature: $T = 298 \text{ K}$



**Fig. 9.** Concentration of five different syngas components at the end of studied period (30 days) in three different porous media: coal, shale and sandstone: (a) Carbon dioxide, (b) Methane, (c) Hydrogen, (d) Carbon monoxide and (e) Nitrogen.

porous media.

In sandstone, gas front of H<sub>2</sub> is located at 18.4 m, further than that of CO<sub>2</sub>, CH<sub>4</sub>, CO and N<sub>2</sub>, which are 16.0 m, 16.3 m, 16.2 m, and 16.0 m, respectively. Similar gas propagation can also be observed in coal and shale. The reason why H<sub>2</sub> propagates further in the domain than other gases is related closely to the gas diffusion coefficients. CO<sub>2</sub>, CH<sub>4</sub>, CO and N<sub>2</sub> have very similar diffusion coefficients:  $1.42 \times 10^{-5} \text{ m}^2/\text{s}$  for CO<sub>2</sub>,  $1.96 \times 10^{-5} \text{ m}^2/\text{s}$  for CH<sub>4</sub>,  $1.9 \times 10^{-5} \text{ m}^2/\text{s}$  for CO, and  $1.5 \times 10^{-5} \text{ m}^2/\text{s}$  for N<sub>2</sub>, while the diffusion coefficient of H<sub>2</sub> ( $6.11 \times 10^{-5} \text{ m}^2/\text{s}$ ) is approximately 5 times higher compared to other gases. It was stated by Nazaroff and Sextro [64] that the importance of gas diffusion increases when the permeability value of porous media is lower than  $1.7 \times 10^{-11} \text{ m}^2$ . Hence, both gas diffusion and advection contribute to the gas transport in these three porous media, but gas

diffusion plays a higher role than gas advection in the cases of coal and shale. Despite one order of magnitude difference in intrinsic permeability values of coal and shale, the location of gas breakthrough fronts differ between 0.4 and 0.9 m, depending on the gas considered. However, it appears that advection and diffusion are competing mechanisms in sandstone as, despite the same porosity of shale and sandstone, gas fronts differ up to 9.2 m.

#### 4.4. Effect of sorption on gas flow

It is observed in Fig. 10a that the gas front of CO<sub>2</sub> in coal is located at round 6.8 m from the injected surface. When gas adsorption is considered, the Langmuir pressure, which is the pressure at which one half of the Langmuir volume can be adsorbed [65], plays an important role



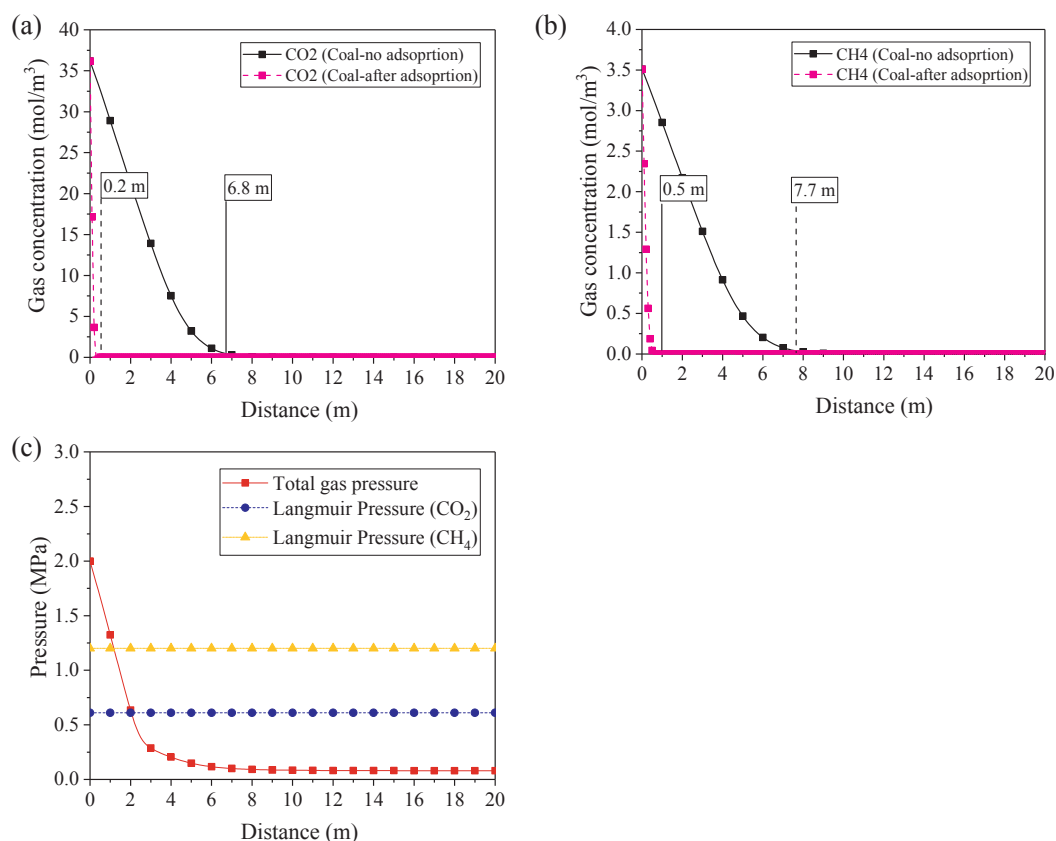


**Fig. 10.** The distribution of gas concentrations in coal with and without considering gas sorption at day 30: (a) Carbon dioxide, (b) Methane and (c) total gas pressure in the case without adsorption.

in the gas distribution. The total gas pressure in the case without adsorption is presented in Fig. 10c. At the injection face, gas pressure is 2.0 MPa, much higher than the Langmuir pressure of CO<sub>2</sub> in coal (0.61 MPa), leading to quick adsorption of CO<sub>2</sub> at a distance of 0.2 m and a very low CO<sub>2</sub> concentration at greater distance from the injection face. In terms of CH<sub>4</sub> (Fig. 10b), its gas front is located at the distance of 7.7 m for the case of non-adsorption and 0.5 m under consideration of adsorption due to the higher total gas pressure at the injection face compared to the Langmuir pressure of CH<sub>4</sub> in coal (1.2 MPa). Therefore, the similar variation tendency of CO<sub>2</sub> can also be identified for CH<sub>4</sub>, presenting the importance of adsorption in the study of gas transport.

The distribution of CO<sub>2</sub> concentrations in shale with and without adsorption is presented in Fig. 11a. The gas front positions in the cases of no adsorption and with considering adsorption are 5.9 m and 0.8 m, respectively. Fig. 11b shows the gas propagation of CH<sub>4</sub> in shale with and without adsorption, allowing a gas front move to 1.8 m and 6.9 m, respectively. It can be observed in Fig. 11c that the total gas pressure (2.0 MPa) is larger than the Langmuir pressure of CO<sub>2</sub> (1.0 MPa) and CH<sub>4</sub> (1.71 MPa) in shale, leading to the efficient adsorption of gases in the first 0.8 m and 1.8 m distances, respectively.

Fig. 12a illustrates the distribution of CO<sub>2</sub> in sandstone with and without consideration of adsorption, presenting the gas fronts located at 1.4 m and 16.0 m, respectively. Langmuir pressure of CO<sub>2</sub> (2.83 MPa) is slightly larger than the total gas pressure at the injection face (Fig. 12c). Thus, CO<sub>2</sub> is absorbed efficiently and its concentration decreases to smaller values at the distance of 1.4 m. However, the Langmuir pressure of CH<sub>4</sub> (3.86 MPa) is larger than the total gas pressure at the injection face, leading to further transport of CH<sub>4</sub>, up to 4.1 m, in sandstone compared to that of CO<sub>2</sub> (Fig. 12b).

As shown above, Langmuir pressure values considered in this study have a strong impact on the amount of adsorbed gases. However, the equilibrium modelling approach taken in this work to consider sorption

also has an impact on the sorbed amount. Using the equilibrium sorption approach, it is assumed that the sorbed amount in the rock matrix is in equilibrium with the free gas concentrations in the pores and fractures [54]. This means that applying a fixed concentration boundary would cause instantaneous sorption at the boundary and reduction of the free gas concentration. However, as gas adsorption is known to be a kinetic reaction, which would include gas exchange between the fractures and the rock matrix, diffusion through the matrix and sorption of the gas molecules on the sorption sites, the equilibrium behaviour is only partially realistic. Implementing a kinetic approach would require further research investigations to obtain a good understanding of the relationship between the adsorbed amount at non-equilibrium conditions for the range of porous media considered in this study. Therefore, the equilibrium approach is adopted for the preliminary study in this paper and provides novel insights into the effect of gas sorption on gas transport.

Another important aspect related to gas sorption is the potential of the host rock to swell under the conditions of gas sorption, which is particularly pronounced in coals compared to shale and sandstone. Swelling of the porous media is understood to be strongly correlated with the sorption amount [66]. The sorption-induced swelling often results in closure of the existing flow paths, thus reducing the permeability of the porous medium and affecting the gas propagation [54]. It would have positive implications for retarding the potential gas escape in the surrounding strata of UCG, especially if there are coal seams located at a certain distance above the UCG reactor which would then act as a barrier. Thereby, considering sorption and rock swelling for UCG surrounding strata would provide a potential not just to retard the gas propagation, but also to provide geological storage of the leaked specific syngas components, such as CH<sub>4</sub> and CO<sub>2</sub>.

As mentioned previously, gas sorption is a temperature dependent process, i.e. the sorption capacity decreases with an increase in

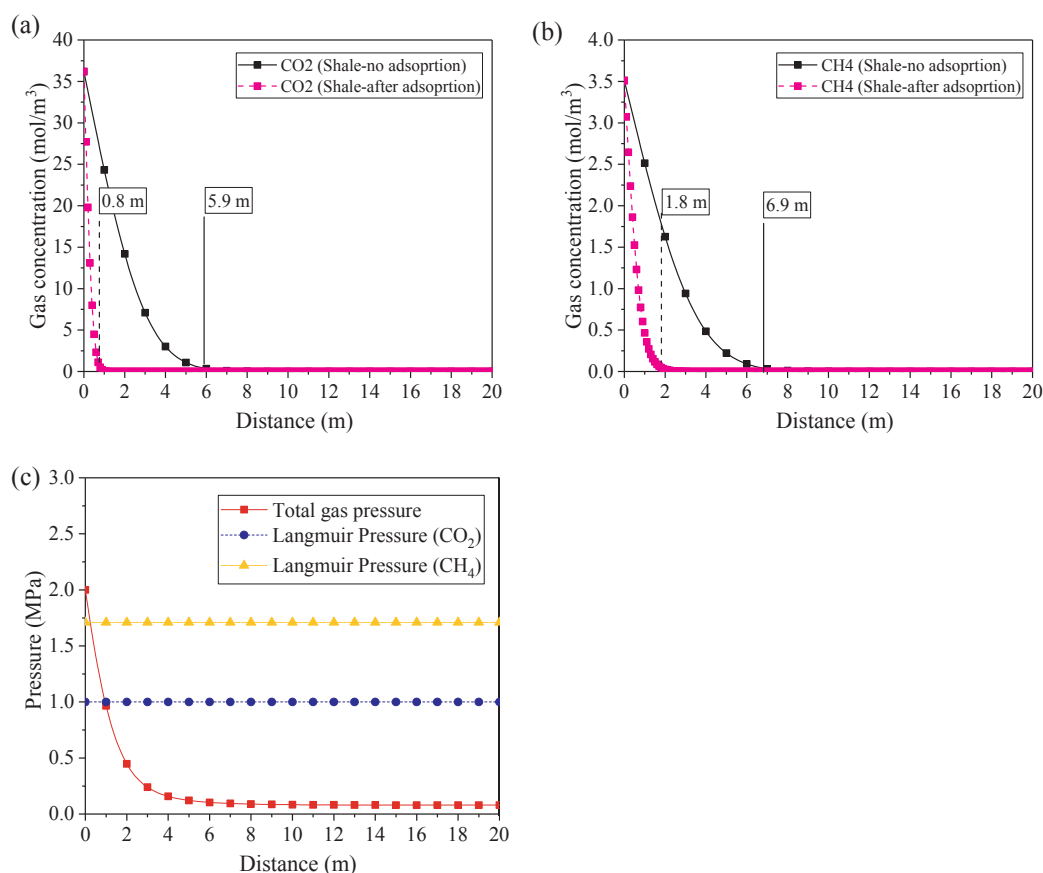


Fig. 11. The distribution of gas concentrations in shale with and without considering the gas sorption at day 30: (a) Carbon dioxide, (b) Methane and (c) total gas pressure in the case without adsorption.

temperature [52]. Hence, future experimental and theoretical studies should be undertaken to provide further understanding on the impact of high temperatures experienced during the UCG process on the sorption potential of the UCG products. In conclusion, the cases with and without consideration of adsorption of  $\text{CO}_2$  and  $\text{CH}_4$  in three different porous media (coal, shale and sandstone) are well analysed depending on their Langmuir isotherms, reflecting the effect of adsorption on the gas propagation and the significance to consider adsorption in the study of gas transport.

## 5. Conclusions

In this study, a thermodynamic equilibrium model is developed and applied to analyse the effect of gasification reagents on the syngas composition and gasification temperature as well as to provide thermal and chemical (gas) boundary conditions for the coupled thermo-chemical model contained within the thermo-hydraulic-chemical-mechanical framework of the COMPASS code. The code is then used to study the variations of temperature and gas concentrations, considering the reactive gas transport mechanisms, in three different porous media (coal, shale and sandstone) surrounding the UCG reactor.

Based on the simulation results on coal gasification conducted under constant pressure conditions (20 bar) and constant air supply (0.5 kmol), it can be concluded that to achieve a syngas with high contents of methane and hydrogen, an excess of steam above the stoichiometric on a molar basis for the primary gasification reactant (e.g. air in this study) is recommended. However, this comes at a potential cost of reducing the overall calorific value of the syngas as the concentration of  $\text{CO}$ , a gas with high calorific value, significantly decreases. Furthermore, higher amounts of steam in the system increase the concentration of  $\text{CO}_2$  in the gas mixture, which poses an environmental

concern and increases the costs associated with  $\text{CO}_2$  utilisation and storage once it is collected at the surface facility.

By studying the transport of a gas mixture under the scenario of a potential gas migration from the UCG reactor into the surrounding strata, it can be inferred that both gas diffusion and advection have a significant role in the gas transport in such low permeable porous media considered in this study. In particular, gas diffusion and advection are competing transport mechanisms in porous media with an intrinsic permeability higher than 1 mD (sandstone), while the gas diffusion becomes a dominant transport process in porous media with an intrinsic permeability lower than 1 mD (coal and shale). Such results confirm the importance of considering low permeability strata surrounding the UCG reactor, widely recognised in the literature [16,46], which can act as an effective barrier to contain the contaminants generated and potentially leaked during the UCG process.

Moreover, the study of gas adsorption of highly potent greenhouse gases, i.e. methane and carbon dioxide by porous media, emphasised the significance of considering the adsorption effect in the gas transport in the overall UCG process. Based on the simulation results presented, it can be concluded that the sorption of gases can retard their propagation in the strata surrounding the UCG cavity which is particularly significant in materials with high affinity to gases, such as coals and shales. Such observations then suggest that the coal pillars separating UCG reactors in a multi-well UCG configuration or shale layers located above the UCG target seams, commonly intersected by thinner coal seams, would adsorb some of the gas that could potentially leak. Although the gas sorption is a temperature-dependent kinetic process which is not fully considered in this work due to the lack of available data, this work provides further insights on the importance of considering the adsorption to understand the gas migration in the area around the UCG reactor.

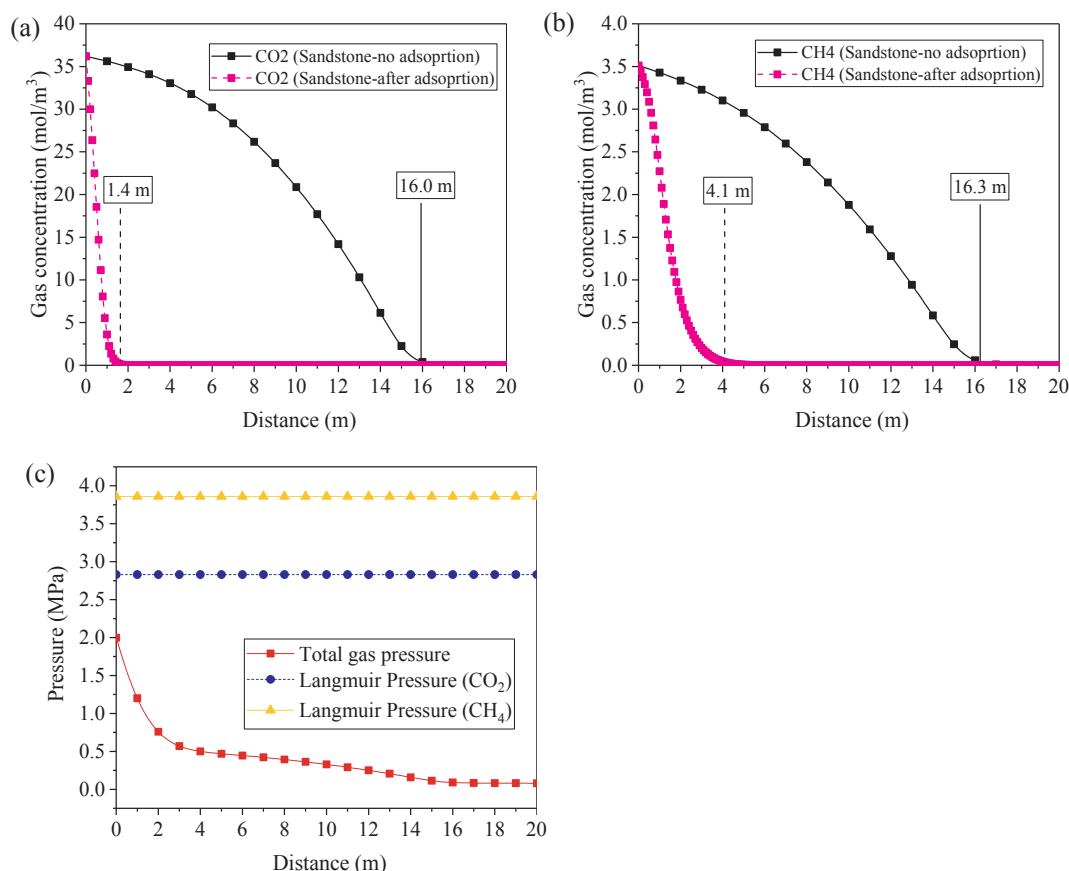


Fig. 12. The distribution of gas concentrations in sandstone with and without considering the gas sorption at day 30: (a) Carbon dioxide, (b) Methane and (c) total gas pressure in the case without adsorption.

With the background of rapid-developed UCG technology and the development of integrated UCG models focusing on syngas production, coal conversion rates and cavity shape, it has been widely suggested that future work should focus on the development of numerical tools capable to simulate and optimise the production and composition of the syngas and the environmental and geo-mechanical impacts of UCG products in complex well configurations [2,3]. Hence, this study contributes to such work by presenting a numerical framework capable of studying the formation of UCG products and its reactive transport in the geological formations surrounding the UCG reactor to address the environmental issues of complicated UCG process, aid in managing the environmental practices, reducing pollution risk and securing greater public and regulatory support for the UCG commercialization.

### Acknowledgements

This work has been carried out as a part of the FLEXIS project part-funded by the European Regional Development Fund through Welsh Government. The financial support, for the first and the second authors, is gratefully acknowledged.

### References

- [1] Bhutto AW, Bazmi AA, Zahedi G. Underground coal gasification: from fundamentals to applications. *Prog Energy Combust Sci* 2013;39(1):189–214.
- [2] Khan MM, et al. Modelling underground coal gasification—a review. *Energies* 2015;8(11):12603–68.
- [3] Perkins G. Underground coal gasification—part II: fundamental phenomena and modeling. *Prog Energy Combust Sci* 2018;67:234–74.
- [4] Andrianopoulos E, Korre A, Durucan S. Chemical process modelling of underground coal gasification and evaluation of produced gas quality for end use. *Energy Procedia* 2015;76:444–53.
- [5] Andrianopoulos E, et al. Coupled Thermo-Mechanical-Chemical modelling of underground coal gasification. *Comput Aided Chem Eng* 2016;1069–74.
- [6] Perkins G, Sahajwalla V. Steady-state model for estimating gas production from underground coal gasification. *Energy Fuels* 2008;22(6):3902–14.
- [7] Perkins G, Sahajwalla V. Modelling of heat and mass transport phenomena and chemical reaction in underground coal gasification. *Chem Eng Res Des* 2007;85(3):329–43.
- [8] Seifi M, Abedi J, Chen Z. Application of porous medium approach to simulate UCG process. *Fuel* 2014;116:191–200.
- [9] Duan T-H, et al. Pyrolysis and gasification modelling of underground coal gasification and the optimisation of CO<sub>2</sub> as a gasification agent. *Fuel* 2016;183:557–67.
- [10] Samdani G, et al. A process model for underground coal gasification—Part-I: cavity growth. *Fuel* 2016;181:690–703.
- [11] Jiang L, Chen Z, Ali SF. Modelling of reverse combustion linking in underground coal gasification. *Fuel* 2017;207:302–11.
- [12] Klebingat S, et al. Innovative thermodynamic underground coal gasification model for coupled synthesis gas quality and tar production analyses. *Fuel* 2016;183:680–6.
- [13] Klebingat S, et al. Optimization of synthesis gas heating values and tar by-product yield in underground coal gasification. *Fuel* 2018;229:248–61.
- [14] Najafi M, Jalali SME, KhaloKakaie R. Thermal-mechanical-numerical analysis of stress distribution in the vicinity of underground coal gasification (UCG) panels. *Int J Coal Geol* 2014;134:1–16.
- [15] Elahi S, Nassir M, Chen Z. Effect of various coal constitutive models on coupled thermo-mechanical modeling of underground coal gasification. *J Petrol Sci Eng* 2017;154:469–78.
- [16] Sury, M., et al. 2004. Review of environmental issues of underground coal gasification. WS Atkins Consultants Ltd., University of Liège Belgium, FWS Consultants Ltd. 126: pp. 1–126.
- [17] Green M. Recent developments and current position of underground coal gasification. *Proc Institution Mech Eng Part A J Power Energy* 2018;232(1):39–46.
- [18] Yang L, Zhang X. Modeling of contaminant transport in underground coal gasification. *Energy Fuels* 2008;23(1):193–201.
- [19] Janoszek T, et al. Modelling of gas flow in the underground coal gasification process and its interactions with the rock environment. *J Sustainable Min* 2013;12(2):8–20.
- [20] Soukup K, et al. Modeling of contaminant migration through porous media after underground coal gasification in shallow coal seam. *Fuel Process Technol* 2015;140:188–97.
- [21] Jiang L, Chen Z, Ali SF. General hydro-geological impact of cleats on underground coal gasification. *Fuel* 2018;224:128–37.
- [22] Imran M, et al. Environmental concerns of underground coal gasification. *Renew Sustain Energy Rev* 2014;31:600–10.

- [23] Liu S-Q, et al. Groundwater pollution from underground coal gasification. *J China Univ Mining Technol* 2007;17(4):467–72.
- [24] Kapusta K, Stańczyk K. Pollution of water during underground coal gasification of hard coal and lignite. *Fuel* 2011;90(5):1927–34.
- [25] Laciak M, et al. The analysis of the underground coal gasification in experimental equipment. *Energy* 2016;114:332–43.
- [26] Kostúr K, Laciak M, Durdan M. Some influences of Underground Coal Gasification on the environment. *Sustainability* 2018;10(5):1512.
- [27] Upadhye R, Burton E, Friedmann J. Science and technology gaps in underground coal gasification. Lawrence Livermore Laboratory: University of California, Livermore, California; 2006. p. 222523.
- [28] Thomas HR, He Y. Modelling the behaviour of unsaturated soil using an elastoplastic constitutive model. *Géotechnique* 1998;48(5):589–603.
- [29] Thomas HR, Sedighi M, Vardon PJ. Diffusive reactive transport of multicomponent chemicals under coupled thermal, hydraulic, chemical and mechanical conditions. *Geotech Geol Eng* 2012;30(4):841–57.
- [30] Hosking LJ, Thomas HR, Sedighi M. A dual porosity model of high-pressure gas flow for geoenery applications. *Can Geotech J* 2017;55(6):839–51.
- [31] Jarunthammachote S, Dutta A. Thermodynamic equilibrium model and second law analysis of a downdraft waste gasifier. *Energy* 2007;32(9):1660–9.
- [32] La Villetta M, Costa M, Massarotti N. Modelling approaches to biomass gasification: a review with emphasis on the stoichiometric method. *Renew Sustain Energy Rev* 2017;74:71–88.
- [33] Thomas H, Cleall P. Inclusion of expansive clay behaviour in coupled thermo hydraulic mechanical models. *Eng Geol* 1999;54(1–2):93–108.
- [34] Zagorščak R, Sedighi M, Thomas HR. Effects of Thermo-Osmosis on Hydraulic Behavior of Saturated Clays. *Int J Geomech* 2016;17(3):04016068.
- [35] Parkhurst DL, Appelo C. 1999. User's guide to PHREEQC (Version 2): a computer program for speciation, batch-reaction, one-dimensional transport, and inverse geochemical calculations.
- [36] Patel VR, Upadhyay DS, Patel RN. Gasification of lignite in a fixed bed reactor: Influence of particle size on performance of downdraft gasifier. *Energy* 2014;78:323–32.
- [37] Zainal Z, et al. Prediction of performance of a downdraft gasifier using equilibrium modeling for different biomass materials. *Energy Convers Manage* 2001;42(12):1499–515.
- [38] Perry RH, Green DW, Maloney JO. Perry's Chemical Engineer's Handbook Chemical Engineer's Handbook. McGraw-Hill; 1984.
- [39] JANAF Thermochemical Tables. Stull, DR and Prophet, H. National Bureau of Standards, Washington, DC: National Standard Reference Data Series; 1971.
- [40] Seetharam S, Thomas H, Cleall PJ. Coupled thermo/hydro/chemical/mechanical model for unsaturated soils—Numerical algorithm. *Int J Numer Meth Eng* 2007;70(12):1480–511.
- [41] Sedighi M, et al. 2014. Geochemical modelling of hydrogen gas migration in an unsaturated bentonite buffer. Geological Society, London, Special Publications 415: p. SP415. 12.
- [42] Fredlund DG, Rahardjo H, Rahardjo H. Soil mechanics for unsaturated soils. John Wiley & Sons; 1993.
- [43] Thomas H, et al. On the development of a model of the thermo-mechanical-hydraulic behaviour of unsaturated soils. *Eng Geol* 1996;41(1–4):197–218.
- [44] Thomas H, He Y, Onofrei C. An examination of the validation of a model of the hydro/thermo/mechanical behaviour of engineered clay barriers. *Int J Numer Anal Meth Geomech* 1998;22(1):49–71.
- [45] Chen M, et al. Dual porosity modelling of the coupled mechanical response of coal to gas flow and adsorption. *Int J Coal Geol* 2019;205:115–25.
- [46] Camp DW, White JA. Underground coal gasification: an overview of groundwater contamination hazards and mitigation strategies. Livermore, CA (United States): Lawrence Livermore National Lab. (LLNL); 2015.
- [47] Hartley A. A depositional model for the Mid-Westphalian A to late Westphalian B Coal Measures of South Wales. *J Geol Soc* 1993;150(6):1121–36.
- [48] Sadasivam S, et al. Baseline geochemical study of the Aberpergwm mining site in the South Wales Coalfield. *J Geochem Explor*, In press.
- [49] Durucan S, et al. Two phase relative permeability of gas and water in coal for enhanced coalbed methane recovery and CO<sub>2</sub> storage. *Energy Procedia* 2013;37:6730–7.
- [50] William E, Airey D. 2005. Influence of stress level on the highly compacted shales in the Sydney Basin. In: Proceedings of the international conference on soil mechanics and geotechnical engineering. AA Balkema Publishers.
- [51] Van Genuchten MT. A closed-form equation for predicting the hydraulic conductivity of unsaturated soils 1. *Soil Sci Soc Am J* 1980;44(5):892–8.
- [52] Gensterblum Y, et al. High-pressure CH<sub>4</sub> and CO<sub>2</sub> sorption isotherms as a function of coal maturity and the influence of moisture. *Int J Coal Geol* 2013;118:45–57.
- [53] Duan S, et al. Adsorption equilibrium of CO<sub>2</sub> and CH<sub>4</sub> and their mixture on sichuan basin shale. *Energy Fuels* 2016;30(3):2248–56.
- [54] Zagorščak R. An investigation of coupled processes in coal in response to high pressure gas injection Ph D. thesis Wales, UK: Cardiff University; 2017.
- [55] Iscan A, Kok M. Porosity and permeability determinations in sandstone and limestone rocks using thin section analysis approach. *Energy Sources Part A* 2009;31(7):568–75.
- [56] Rodrigues C, De Sousa ML. The measurement of coal porosity with different gases. *Int J Coal Geol* 2002;48(3–4):245–51.
- [57] Yang YaA, A.C.. A permeability–porosity relationship for mudstones. *Mar Petroleum Geol* 2010;27(8):1692–7.
- [58] Akinlotan O. Porosity and permeability of the English (Lower Cretaceous) sandstones. *Proc Geol Assoc* 2016;127(6):681–90.
- [59] Li H, Guo G, Zheng N. High-temperature effects of the surrounding rocks around the combustion space area in SMFM-CRIP—a case study in China. *Energy Sources Part A* 2018;40(17):2021–36.
- [60] Tang F, et al. Thermophysical properties of coal measure strata under high temperature. *Environ Earth Sci* 2015;73(10):6009–18.
- [61] Kosowska-Golachowska M, Gajewski W, Musiał T. Determination of the effective thermal conductivity of solid fuels by the laser flash method. *Arch Thermodynamics* 2014;35(3):3–16.
- [62] Fujii T, et al. Evaluation of CO<sub>2</sub> sorption capacity of rocks using a gravimetric method for CO<sub>2</sub> geological sequestration. *Energy Procedia* 2009;1(1):3723–30.
- [63] Bashir H. Methane adsorption into sandstones and its role in gas recovery from depleted reservoirs. University of Salford; 2018.
- [64] Nazaroff WW, Sextro RG. Technique for measuring the indoor radon-222 source potential of soil. *Environ Sci Technol* 1989;23(4):451–8.
- [65] Busch A, Gensterblum Y. CBM and CO<sub>2</sub>-ECBM related sorption processes in coal: a review. *Int J Coal Geol* 2011;87(2):49–71.
- [66] Day S, et al. Swelling of coals by supercritical gases and its relationship to sorption. *Energy Fuels* 2010;24(4):2777–83.